Broadband Linearly Polarized Beat-Wave TE_{m1}/TE_{11} Mode Converters

D. B. McDermott, J. Pretterebner, C. K. Chong, C. F. Kinney, M. M. Razeghi, and N. C. Luhmann Jr.

Abstract—**Broadband linearly polarized waveguide mode converters have been developed to transform the high-order cylindrical TE_{m1} output wave from harmonic gyrotron amplifiers into the more useful TE_{11} fundamental waveguide mode. The converter's corrugation period is equal to the beat between the two waves and the bandwidth is predicted to be inversely proportional to the number of periods. Four-period TE_{31}/TE_{11} and TE_{41}/TE_{11} converters with an azimuthal perturbation of $m_c = 4$ and $m_c = 5$, respectively, have yielded a peak conversion efficiency of 98% with a bandwidth greater than 3% and a one-period beat-wave converter has been designed to yield 12% bandwidth. However, it has been observed in measurements that the strong coupling in a short converter can lead to a shift of the center-frequency with an accompanying reduction of the efficiency and bandwidth. A two-period TE_{41}/TE_{11} converter with 5% bandwidth displayed a 5% frequency shift and a conversion efficiency of only 86%.**

I. Introduction

THERMIONIC FAST-WAVE AMPLIFIERS [1]–[7] are often designed to generate their rf output in a high order mode. It is usually desirable to transform the electromagnetic energy into the lowest order mode of the transmission system. Corrugated beat-wave mode converters [8]–[10], which have been developed by the fusion plasma community for electron cyclotron resonance heating (ECRH) [11]–[13] of magnetic fusion reactors, can in principle selectively transform any mode into any other mode. The principle of operation in this three-wave process is to use the zero-frequency corrugation "idler wave" to resonantly transfer the energy in one electromagnetic mode to another. A wave of frequency ω that is initially in a mode with the azimuthal and radial eigennumbers (m_i, n_i) with wavevector β_i can be transferred into mode (m_f, n_f) with wavector β_f if the period ℓ_c and azimuthal multipole m_c of the converter's corrugation satisfies the beat conditions, $m_f = m_i \pm m_c$ and $\beta_f = \beta_i \pm \beta_c$, where $\beta_c = 2\pi/\ell_c$. The conversion efficiency can theoretically reach unity and has exceeded 99% in practice [9]. Some energy will be transferred into spurious waves that do not satisfy the above beat conditions, but their generation is limited by destructive interference.

The bandwidth has not been a concern for the mode converters designed for ECRH since the typical high power gyrotron source is a fixed frequency oscillator. However, for the application of transforming the high-order output wave from an overmoded fast-wave amplifier, the bandwidth of the mode converter should be at least as wide as that of the amplifier. The required broad bandwidth can be realized from a short converter. It has been shown [9] that a beat-wave converter's bandwidth is approximately inversely proportional to the number of periods. The mode converters reported in this paper were developed to transform the linearly polarized cylindrical TE_{m1} waves generated by a slotted mth-harmonic gyrotron traveling-wave tube (gyro-TWT) amplifier with ~3% bandwidth into the more useful fundamental TE_{11} mode. The usual convention that m is a positive integer or zero will be used.

Beat-wave converters for ECRH are usually circularly polarized. A linearly polarized converter can be created by superimposing the corrugation pattern of two oppositely wound circularly polarized converters as shown in Fig. 1. To transform an mth-order azimuthal mode into a first-order mode, the converter can have either an $m_c = m + 1$ or $m_c = m - 1$ azimuthal multipole geometry. The choice of $m_c = m + 1$ yields better selectivity because the mode numbers of the spurious generated waves are more widely separated and the converter can be designed so that more of these higher order, spurious modes are cutoff. Fig. 2 shows the mode selection rule for an $m_c = m + 1$ converter acting on the two circularly polarized components of a linearly polarized TE_{m1} wave to create a linearly polarized TE_{11} wave. In the inverse process, which occurs simultaneously in the resonant transfer process, the TE_{11} wave converts back into the TE_{m1} mode and also into either the $TE_{m+2,1}$ mode for $m_c = m+1$ or the $TE_{m-2,1}$ mode for $m_c = m - 1$. The excitation of $TE_{m+2,1}$ waves can be suppressed by choosing the radius to be sufficiently narrow to cut off this mode. However, the TE_{m1} converter with $m_c = m - 1$ will not cutoff the $TE_{m-2,1}$ waves it generates. Although this spurious wave does not satisfy the wavevector matching condition, its generation represents a loss of energy and should be avoided.

The organization of this paper is as follows. The theory used to predict the behavior of corrugated beat-wave mode converters is presented in Section II. This theory was used to design four broadband TE_{m1}/TE_{11} converters. After describing the diagnostic system, the measurements of three of these

Manuscript received June 11, 1995, revised November 12, 1995. This work was supported in part by the U.S. AFOSR Grants F49620-94-1-0426 (Tri-Services) and F49620-92-J-0175, and Contract F30602-94-2-0001 (ATRI), by the U.S. ARO Contract DAAH04-93-G-0084, and by Varian Subcontract 109BAR05943 ARPA-DSO Contract N00014-91-C-2221.

D. B. McDermott, C. K. Chong, M. M. Razeghi, and N. C. Luhmann Jr. are with the Department of Applied Science, University of California, Davis, CA 95616 USA.

J. Pretterebner is with Innovative Microwave Technology, GmbH, Stuttgart, Germany.

C. F. Kinney is with CPI/Varian Associates, Inc., Palo Alto, CA 94304 USA.

Publisher Item Identifier S 0018-9480(96)01453-6.

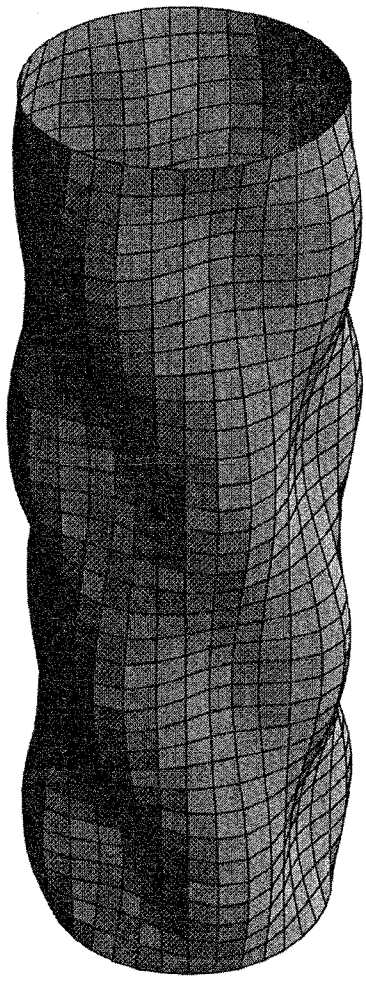

Fig. 1. Schematic of a two period, linearly polarized beat-wave TE_{31}/TE_{11} mode converter.

converters are compared in Section III to the predictions from theory. The dependence of an observed center-frequency shift on the number of periods is also discussed. Section IV contains the final discussion and summary.

II. Theory

The inner radius of a linearly polarized converter in cylindrical waveguide is prescribed by

$$r(\theta, z) = r_w + a\xi(\theta, z) \tag{1}$$

where r_w is the mean radius, a is the amplitude of the corrugation, and $\xi(\theta, z)$ is the geometrical form function of the perturbation which is specified by

$$\xi(\theta, z) = \cos(m_c\theta + \beta_c z) + \cos(m_c\theta - \beta_c z) \tag{2}$$

which can also be written as

$$\xi(\theta, z) = 2\cos(m_c\theta)\cos(\beta_c z). \tag{3}$$

An electromagnetic wave with frequency ω can progagate through a waveguide as an infinite sum of TE and TM modes. A perturbation of the wall will intercouple the wave

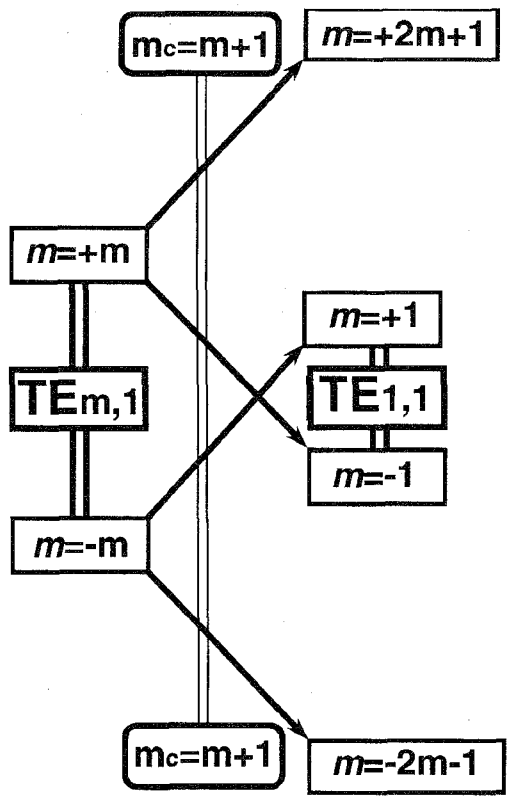

Fig. 2. Diagram showing the transformation of the circularly-polarized components of a linearly polarized TE_{m1} mode into the circularly-polarized components of a linearly polarized TE_{11} mode in a linearly polarized converter with $m_c = m + 1$.

components. For a weak perturbation, the complex amplitude for each coupled traveling wave satisfies

$$\frac{d}{dz}A_i(z) = -\gamma_i A_i(z) + \xi(\theta, z)\sum_{k\neq i} K_{ik}A_k(z) \tag{4}$$

where $\gamma_i = \alpha_i + j\beta_i$, α_i is the attenuation for each wave, β_i is its propagation constant, and K_{ij} are the coupling coefficients between the two modes i and j. The coupling coefficients for sinusoidal corrugation are given [14] by

$$K_{ik} = \frac{a}{2r_w^3}\frac{\left(-x_{mn}^2 x_{m'n'}^2 + mm' r_w^2(\omega^2/c^2 + \beta\beta')\right)}{\left((\beta\beta')\left(x_{mn}^2 - m^2\right)\left(x_{m'n'}^2 - m'^2\right)\right)^{1/2}} \tag{5}$$

for the coupling of TE_{mn} and $TE_{m'n'}$ modes

$$K_{ik} = \frac{a}{2r_w}\frac{(\omega^2/c^2 + \beta\beta')}{(\beta\beta')^{1/2}} \tag{6}$$

for the coupling of TM_{mn} and $TM_{m'n'}$ modes, and

$$K_{ik} = \frac{a}{2r_w}\frac{m(\omega/c)(\beta + \beta')}{\left((\beta\beta')\left(x_{mn}^2 - m^2\right)\right)^{1/2}} \tag{7}$$

for the coupling of TE_{mn} and $TM_{m'n'}$ modes.

Although the full multimode set of equations (4) should be used to check a design for efficient conversion into a single mode, a two-mode theory can be used to obtain the approximate conversion length and bandwidth. If the attenuation of

TABLE I
PARAMETERS OF FOUR TE_{m1}/TE_{11} MODE CONVERTERS.

	(a) TE_{21}/TE_{11} One-period	(b) TE_{31}/TE_{11} Four-period	(c) TE_{31}/TE_{11} Two-period	(d) TE_{41}/TE_{11} Four-period
center frequency	95.01 GHz	10.24 GHz	10.24 GHz	10.31 GHz
m_c	3	4	4	5
ω/ω_c	1.20	1.24	1.24	1.30
corrugation amplitude, a	0.267 mm	0.99 mm	2.00 mm	1.549 mm
mean diameter, $2r_w$	3.668 mm	48.62 mm	48.62 mm	64.01 mm
beat length, ℓ_c	10.005 mm	85.45 mm	85.45 mm	89.56 mm
total length	10.005 mm	341.80 mm	170.90 mm	358.24 mm
analytical optimum length	10.007 mm	354.7 mm	175.6 mm	301.7 mm

the two waves and the generation of spurious modes can both be neglected, the coupled transmission line equations [10] for the two principal waves are

$$\frac{d}{dz}A_1(z) = -j\beta_1 A_1(z) + 2\cos(m_c\theta)\cos(\beta_c z)K_{12}A_2(z) \tag{8}$$

and

$$\frac{d}{dz}A_2(z) = -j\beta_2 A_2(z) + 2\cos(m_c\theta)\cos(\beta_c z)K_{21}A_1(z). \tag{9}$$

After multiplying the wave amplitudes by $\exp(\pm j\beta_c z/2)$, as appropriate, to transform both waves into the same "center" frame, recognizing that the coupling coefficients are symmetric, and then ignoring the fast oscillation terms, the solution for the two waves can be found as

$$A_1(z) = \left[\cos\left(\frac{z}{2}\sqrt{\delta^2 + K_{12}^2}\right) + j\frac{\delta}{\sqrt{\delta^2 + K_{12}^2}} \times \sin\left(\frac{z}{2}\sqrt{\delta^2 + K_{12}^2}\right)\right]e^{-j\beta_1 z} \tag{10}$$

and

$$A_2(z) = \frac{K_{12}}{\sqrt{\delta^2 + K_{12}^2}}\sin\left(\frac{z}{2}\sqrt{\delta^2 + K_{12}^2}\right)e^{-j\beta_2 z} \tag{11}$$

where $\delta = \beta_1 - \beta_2 - \beta_c$ is the mismatch. This solution is in the same form as obtained [15] for tight coupling of two transmission lines. For exact resonance ($\delta = 0$), these equations predict that the power will be cyclically transferred [10] in a length of

$$L_{\text{opt}} = \frac{\pi}{K_{12}}. \tag{12}$$

The bandwidth can also be obtained from these equations. It is seen from (10) and (11) that the mismatch to achieve a particular condition scales with the coupling strength. The wavevector mismatch for 90% power transfer in a converter of length L_{opt} can be found to satisfy $\delta = K_{12}/\pi$. By subtracting the wave equations for the initial and final waves at exact resonance from the two wave equations at the mismatch edges, the bandwidth for 90% power transfer can be found to approximately be

$$\frac{\Delta\omega}{\omega} = \frac{1}{\pi N}\left(\frac{\beta_1}{\beta_0}\right)\left(\frac{\beta_2}{\beta_0}\right) \tag{13}$$

where N is the number of beat-periods in the converter and $\beta_0 = \omega/c$. Throughout this paper, the bandwidth will be defined as the normalized width between the two frequencies that yield 90% of the maximum power transfer.

The two-mode theory was used to design a broadband, linearly polarized, $m_c = 3$, TE_{21}/TE_{11} mode converter for a 0.5 MW, 94 GHz, second-harmonic gyro-TWT amplifier [3], whose output is in the TE_{21} mode. The converter's bandwidth needed to be much broader than the amplifier's predicted bandwidth of 7%. An $m_c = 3$ converter was designed with a length of only one beat-period and a bandwidth of 15.1% as predicted by (12). The parameters are shown in Table I(a). Since the center frequency was chosen to be only 20% above the cutoff frequency for the TE_{21} mode, the only other modes that can propagate are the TE_{11} and TM_{01}, of which only the TE_{11} mode satisfies the azimuthal matching condition. Therefore, spurious mode generation was not expected to be a problem. However, since the cutoff frequency of the TM_{11} mode is at the upper end of the bandwidth, the full multimode set of equations (4) were used to evaluate the converter. The spatial evolution of a wave initially in the TE_{21} mode is shown in Fig. 3. The maximum transfer to the TE_{11} mode occurs for a length of 1.00 cm, which agrees within 0.02% to the optimal length predicted by the two-mode analytical theory. The peak conversion efficiency is 99.85% and occurs 2.3% below the design frequency. The ohmic loss in ideal copper is only 0.33%. The converter's bandwidth from the simulation is shown in Fig. 4. The bandwidth is reduced from the analytical value (12) on the low frequency end by dispersion and on the high frequency end by the onset of the TM_{11} mode. Still, the predicted bandwidth of 11.5% is much broader than needed for the amplifier application.

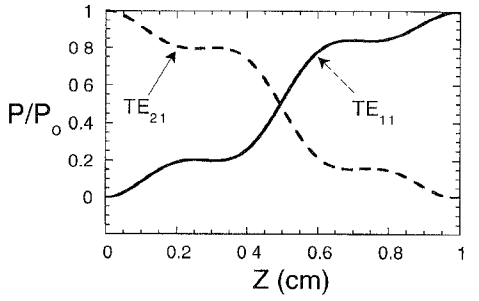

Fig 3. Spatial dependence of power distribution in the TE_{21} (dashed line) and TE_{11} (solid line) modes from simulation for a 93 GHz wave in the one-period TE_{21}/TE_{11} converter (Table I(a), TE_{21} input)

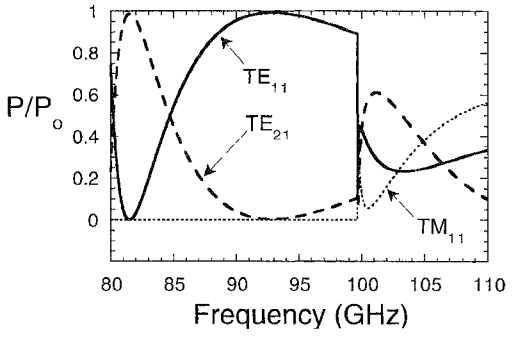

Fig. 4. Dependence on frequency of power distribution in the TE_{21} (dashed line), TE_{11} (solid line), and TM_{11} (dotted line) modes from simulation for the wave emanating from the one-period $m_c = 3$ converter (Table I(a)) and normalized to power of the TE_{21} input wave.

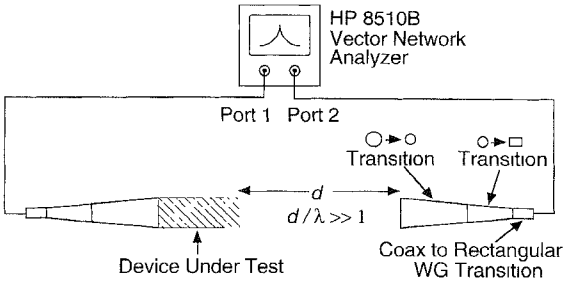

Fig. 5. Schematic of experimental configuration to measure the insertion loss through the beat-wave TE_{m1}/TE_{11} mode converters.

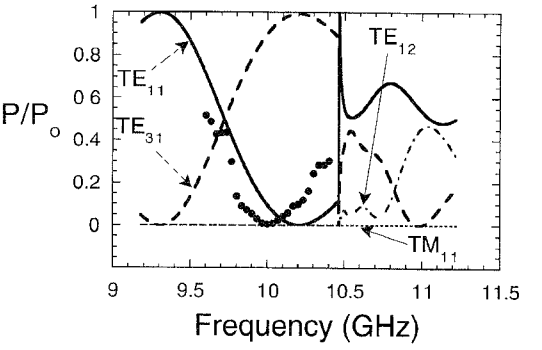

Fig 6. Dependence on frequency of power distribution in the TE_{11} (solid line), TE_{31} (dashed line), TM_{11} (dotted line), and TE_{12} (dot-dashed line) modes from simulation and in the TE_{11} mode from measurement (solid circles) of the wave emitted from the four-period $m_c = 4$ converter (Table I(b)) and normalized to power of the TE_{11} input wave.

III. Measurement

Several broadband linearly polarized beat-wave TE_{m1}/TE_{11} mode converters have been built. Each converter was fabricated by electroforming copper over an aluminum mandril that was then etched away. The configuration of the measurement system based upon a Hewlett-Packard 8510 Automated Vector Network Analyzer is shown in Fig. 5. The converter is connected to the coaxial transmission line of the Network Analyzer's port 1 through an adapter comprised of a circular to circular waveguide taper transition, a circular to rectangular waveguide transition and a rectangular waveguide to coaxial cable transformer. In this way, the Network Analyzer launches a TE_{11} mode into the converter. To receive the TE_{11} mode transmitted by the converter, an identical adapter is positioned along the same axis with a one meter gap separation and attached to port 2 of the Network Analyzer. The purpose of including a gap in the Analyzer's transmission path is to avoid trapping higher order modes by radiating them out of the path. Configured in this way, the S_{21} insertion loss measurement finds the power remaining in the TE_{11} mode. Except for the generation of spurious modes, the properties of conversion from TE_{m1} to TE_{11} are identical to the inverse process of conversion from TE_{11} to TE_{m1}. Reciprocity is guaranteed from the symmetry of the two-mode equations (8) and (9) and their solution (10) and (11).

The four-period converter with an azimuthal symmetry of $m_c = 4$ described in Table I(b) was designed to transform the TE_{31} output of a 3% bandwidth, slotted third-harmonic gyro-TWT [4] and [5] into the TE_{11} mode. The bandwidth of the converter from simulation and measurement is shown in Fig. 6. Although the measured bandwidth of 3.3% agrees fairly well with the 4.3% value predicted by the multimode theory as well as the 4.4% value predicted by the two-mode theory, it is evident that the center frequency has shifted by -2.5% from the design value and -2.2% from the simulation value. The simulation indicates that the excitation of the TE_{12} mode can be quite destructive to the desired conversion process above its cutoff at 10.47 GHz, which was designed to be above the converter's primary bandwidth. The converter had been built in sections so that the conversion could be monitored as a function of distance. The length of the sections are multiples of one-half of the beat period. By referring to the geometrical form function of the corrugation in (3) or by directly viewing the converter in Fig. 1, it can be realized that the crosssection of the converter is a perfect circle every half period. The converter sections end at these positions. The spatial dependence of a TE_{11} wave in the converter from measurement and simulation is shown in Fig. 7. The spatial transformation of the measured center-frequency wave agrees well with the predicted (4) transformation of the predicted center frequency. For a conversion length of four periods, the power remaining in the TE_{11} mode at the center frequency was predicted to be 0.34% and the measured value was 0.005%. The pattern of the converted wave was measured using the Network Analyzer with an azimuthally rotatable radial probe near the wall of the output circular waveguide and is shown

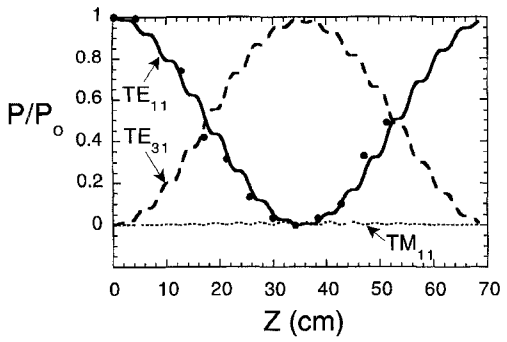

Fig. 7. Spatial dependence of power distribution in the TE_{11} (solid line), TE_{31} (dashed line), and TM_{11} (dotted line) modes from simulation for a 10.2 GHz wave in the four-period TE_{31}/TE_{11} converter (Table I(b)) and in the TE_{11} mode from measurement (solid circles) for a 10.0 GHz wave (TE_{11} input).

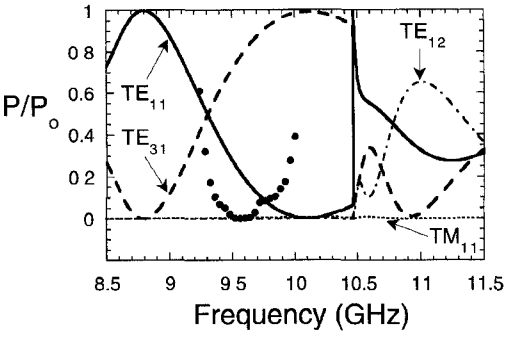

Fig. 9. Dependence on frequency of power distribution in the TE_{11} (solid line), TE_{31} (dashed line), TM_{11} (dotted line), and TE_{21} (dot-dashed line) modes from simulation and in the TE_{11} mode from measurement (solid circles) of the wave emitted from the two-period $m_c = 4$ converter (Table I(c)) and normalized to power of the TE_{11} input wave.

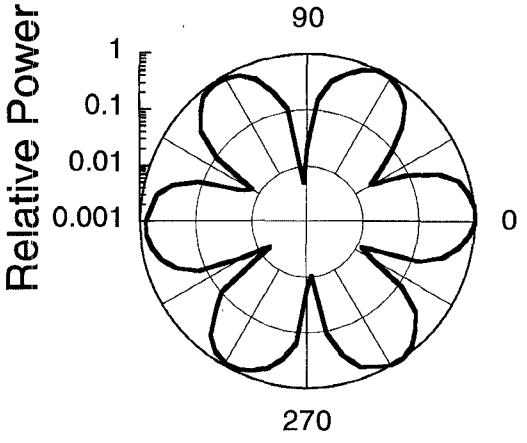

Fig. 8. Measured azimuthal dependence of the radial electric field of a 10.0 GHz wave after propagating through the four-period TE_{31}/TE_{11} converter (Table I(b), TE_{11} input).

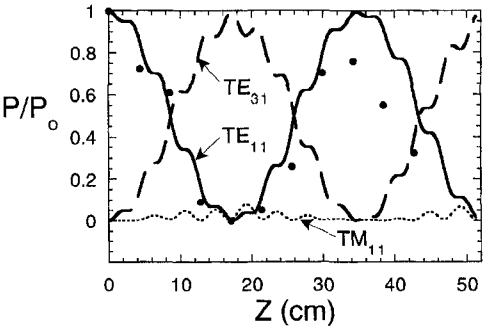

Fig. 10. Spatial dependence of power distribution in the TE_{11} (solid line), TE_{31} (dashed line), and TM_{11} (dotted line) modes from simulation for a 10.1 GHz wave in the two-period TE_{31}/TE_{11} converter (Table I(c)) and in the TE_{11} mode from measurement (solid circles) for a 9.6 GHz wave (TE_{11} input).

in Fig. 8. Although the pattern suggests that the converted wave is a fairly pure third-order azimuthal mode, the purity is somewhat reduced when the probe's lower sensitivity ($\div 2.8$) to the radial electric field of the TM_{11} volume mode is included. Whereas the multimode theory predicted that the mode distribution of the center-frequency wave would be 99.9% in the TE_{31} mode, the purity of the converted wave is actually 98.4%. Including the spurious mode generation and the predicted attenuation of 0.47% using a resistivity twice that of ideal copper, the maximum efficiency of the converter is 97.9%.

In an attempt to further increase the converter's bandwidth for the gyro-TWT application, a shorter TE_{31}/TE_{11} converter was built. Fig. 9 shows the bandwidth of the two-period converter summarized in Table I(c). The center frequency has shifted significantly from the design value (-4.9%) and the simulation value (-6.3%). Also, the measured bandwidth of 5.2% is considerably less than the multimode prediction of 7.1% and the two-mode prediction of 8.8%. Concerning the generation of spurious modes as predicted by simulation, the TM_{11} mode is excited to a higher level than in the four-period model and the TE_{12} mode again becomes an impediment above its cutoff at 10.47 GHz. The two-period converter was also built in sections so that the spatial dependence of the conversion could be followed. Fig. 10 shows the spatial history of a TE_{11} wave at the measured center frequency compared to the simulated behavior of the predicted center-frequency wave. The wave follows the predicted behavior in the initial stages of the converter, but diverges progressively more in the later stages. Evidently, a significant fraction of the initial energy converts into modes that do not reform back into the TE_{11} mode. The resonant transfer has been broken. For a conversion length of two periods, the power remaining in the TE_{11} mode at the center frequency was measured to be only 0.05%, which is to be compared with the 0.2% value predicted by the multimode theory. However, it is evident in the mode pattern in Fig. 11 that all of this energy did not transfer into the TE_{31} mode. Whereas the multimode theory predicted that the mode distribution of the converted wave at the center frequency would be 99.8% in the TE_{31} mode, the converted wave is found to actually be only 86.4% in the desired mode using a probe sensitivity ratio of 3.3. The peak efficiency of this converter is 86.1%.

A third converter with an azimuthal symmetry of $m_c = 5$ and summarized in Table I(d) was built to transform the TE_{41} output of a 3% bandwidth, slotted third-harmonic peniotron-TWT amplifier [6] and [16] into the TE_{11} mode. The bandwidth of the four-period $m_c = 5$ converter is shown in Fig. 12, where the corrugation amplitude used in the simulation code is

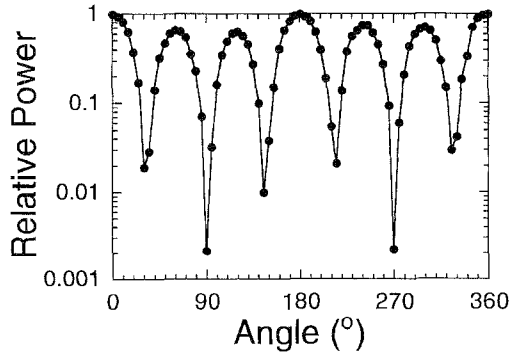

Fig. 11 Measured azimuthal dependence of the radial electric field of a 9 6 GHz wave after propagating through the two-period TE_{31}/TE_{11} converter (Table I(c), TE_{11} input).

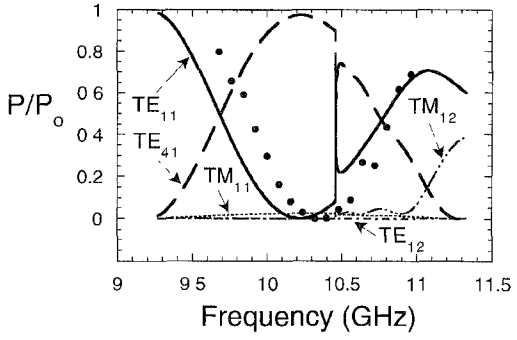

Fig. 12. Dependence on frequency of power distribution in the TE_{11} (solid line), TE_{41} (dashed line), TM_{11} (dotted line), TE_{12} (dot-dashed line) and TM_{12} (dot-dot-dot-dashed line) modes from simulation and in the TE_{11} mode from measurement (solid circles) of the wave emitted from the four-period $m_c = 5$ converter (Table I(d)) and normalized to power of the TE_{11} input wave

equal to the optimum value from the two-mode theory (12) for the four-period length. The center frequency shift of $+0.4\%$ from the design and $+1.2\%$ from the simulation prediction is much less than in the four-period $m_c = 4$ converter and is in the opposite direction. The measured bandwidth of 3.5% is to be compared with the 4.6% value predicted by the multimode theory as well as the 4.9% value predicted by the two-mode theory. The power remaining in the TE_{11} mode at the center-frequency was measured to be 0.03%, which agrees well with the predicted value of 0.04%. The radial probe measurement of the converted wave in Fig. 13 shows that a high purity fourth-order azimuthal mode has been generated. Whereas the multimode theory predicted that the mode distribution of the center-frequency wave would be 97.5% in the TE_{41} mode (2.5% in the TM_{11} mode), the actual TE_{41} content of the converted wave was measured to be 98.4%. The probe's higher sensitivity ($\times 2.46$) to the TE_{41} surface mode compared to the TM_{11} mode has been included. From the simulation results in Fig. 12, the TE_{12} level remains under 0.013% over the bandwidth of interest, and the onset of the TM_{12} mode at 10.48 GHz does not have nearly as sever an effect as the TE_{12} mode has in the $m_c = 4$ converters. Including the nonideal effects of spurious mode generation, attenuation and incomplete power transfer, the maximum efficiency of the four-period $m_c = 5$ converter was still found to reach 98.4%.

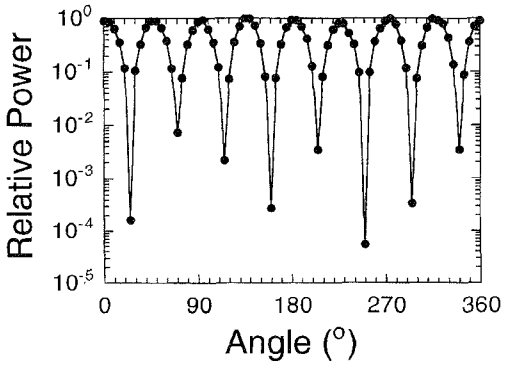

Fig. 13. Measured azimuthal dependence of the radial electric field of a 10.3 GHz wave after propagating through the four-period TE_{41}/TE_{11} converter (Table I(d), TE_{11} input).

IV. Summary

Beat-wave mode converters can been used to transform the high-order linearly polarized TE_{m1} output from broadband fast-wave amplifiers into the fundamental TE_{11} mode. Using the theory reviewed in Section II, several converters were designed and tested. Since the center frequency of the four-period TE_{41}/TE_{11} converter did not shift significantly (0.4%), it yielded the best performance. Its efficiency was 98.4% with a 3.5% bandwidth. The four-period TE_{31}/TE_{11} converter yielded an efficiency of 97.9% with a 3.3% bandwidth and a 2.5% shift of its center frequency. Although the four-period converters' bandwidth marginally satisfies the 3% bandwidth requirement for the amplifier application, it is apparent that the bandwidth is limited from being increased much further. Although the bandwidth is analytically predicted to be inversely proportional to the number of periods, the increased shift of the center frequency from the stronger coupling required for a shorter converter leads to increased mode impurity and a reduction of the bandwidth. The two-period TE_{41}/TE_{11} converter yielded only 86.1% conversion efficiency with 5.2% bandwidth due to the 5.0% strong coupling frequency shift. Converters with broader bandwidth should be designed using the full Maxwell's equations in order to account for the strong coupling effects. By proper compensation, the 11.5% bandwidth predicted for the 95 GHz, one-period TE_{21}/TE_{11} converter should be achievable, especially since it does not generate spurious modes.

References

[1] Y. Y. Lau and L. R. Barnett, "Theory of a low magnetic field gyrotron (gyromagnetron)," *Int. J Infrared and Millimeter Waves*, vol 3, pp 619–643, 1982.

[2] H. Guo, D. S Wu, G. Liu, Y. H. Miao, S. Z. Qian, and W. Z. Qin, "Special complex open-cavity and low magnetic-field high-power gyrotron," *IEEE Trans Plasma Sci.*, vol. 18, pp. 326–333, 1990.

[3] Q. S. Wang, D. B. McDermott, C S Kou, A T Lin, K R Chu, and N. C. Luhmann Jr., "High-power harmonic gyro-TWT's—Part II Nonlinear theory and design," *IEEE Trans Plasma Sci.*, vol 20, no. 3, pp 163–169, 1992

[4] C. K. Chong, D. B. McDermott, A J. Balkcum, and N C Luhmann Jr., "Nonlinear analysis of high-harmonic slotted gyro-TWT amplifier," *IEEE Trans. Plasma Sci.*, vol. 20, no. 3, pp. 176–187, 1992.

[5] W. DeHope, K. Felch, G. Hu, M Mizuhara, J. Neilson, P. Reysner, R. Schumacher, B Stockwell, A. Balkcum, C Chong, N. Luhmann Jr., and

D. McDermott, "Initial tests of a high power, broadband gyro-TWT," in *Tech. Dig. Int. Electron Devices Meet.*, 1993, pp. 355–358.
[6] A. K. Ganguly, S. Ahn, and S. Y. Park, "Three dimensional nonlinear theory of the gyropeniotron amplifier," *Int. J. Electron.*, vol. 65, no. 3, pp. 597–618, 1988.
[7] G. Döhler, D. Gallagher, J. Richards, and F. Scafuri, "Harmonic high power 95 GHz peniotron," in *Tech. Dig. Int. Electron Devices Meet.*, 1993, pp. 363–366.
[8] N. F. Kovalev, I. M. Orlova, and M. I. Petelin, "Wave transformation in a multi-mode waveguide with corrugated walls," *Izv. Vyssh. Ucheb. Zaved. Radiofiz.*, vol. 11, pp. 783–786, 1968; and *Radio Phys. Quant. Electron.*, vol. 11, pp 449–450, 1969.
[9] C. Moeller, "Mode converters used in the doublet III ECH microwave system," *Int. J. Electron.*, vol. 53, no. 6, pp. 587–393, 1982.
[10] M. Thumm, "High-power millimeter-wave mode converters in over-moded circular waveguides using periodic wall perturbations," *Int. J. Electronics*, vol. 57, no. 6, pp. 1225–1246, 1984.
[11] R. M. Gilgenbach, M. E. Read, K E. Hackett, R. Lucey, B. Hui, V. L. Granatstein, K. R. Chu, A. C England, C. M. Loring, O. C. Eldridge, H. C. Howe, A. G. Kulchar, E. Lazarus, M. Murakami, and J. B. Wilgen, "Heating at the electron cyclotron frequency in the ISX-B tokamak," *Phys. Rev. Lett.*, vol. 44, pp. 647–650, 1980.
[12] C. P. Moeller, V. S. Chan, R. J. La Haye, R. Prater, T. Yamamoto, A. Funahashi, K. Hoshino, and T. Yamouchi, "Electron cyclotron heating experiments on the JFT-2 tokamak using an inside launch antenna," *Phys. Fluids*, vol. 25, pp. 1211–1216, 1982.
[13] R. Wilhelm, G. Janzen, G. Müller, P. G. Schuller, K. Schwörer, M. Thumm, and V. Erckmann, "First ECRH-experiments on the W VII-A stellerator," *Plasma Phys. Controlled Fusion*, vol. 26, pp. 259–261, 1984.
[14] G. G. Denisov and M. G. Reznikov, "Corrugated cylindrical resonators for short-wavelength relativistic microwave oscillators," *Izv. Vyssh. Ucheb. Zaved. Radiofiz.*, vol. 25, no. 5, pp. 562–569, 1982.
[15] S. E. Miller, "Coupled wave theory and waveguide applications," *Bell Syst. Tech. J.*, vol. 33, pp. 661–719, 1954.
[16] A. T. Lin, C. K. Chong, D. B. McDermott, A. J. Balkcum, F. V. Hartemann, and N. C. Luhmann Jr., "Slotted third-harmonic peniotron forward-wave oscillator," in *Proc. of SPIE Conf. Intense Microwave Pulses*, 1994, vol. 2154, pp. 327–332.

D. B. McDermott, photograph and biography not available at the time of publication.

J. Pretterebner, photograph and biography not available at the time of publication.

C. K. Chong, photograph and biography not available at the time of publication.

C. F. Kinney, photograph and biography not available at the time of publication.

M. M. Razeghi, photograph and biography not available at the time of publication.

N. C. Luhmann Jr., photograph and biography not available at the time of publication.